

Variation of structural and magnetic properties of $\text{Ni}_{0.1}\text{Mn}_{0.4}\text{Cu}_{0.2}\text{Cd}_{0.3}\text{Fe}_2\text{O}_4$ prepared by sol-gel auto combustion process

M. Moazzam Hossen^{1*}

¹Department of Computer Science & Engineering, International Islamic University Chittagong, Chattogram-4318, Bangladesh.

Abstract: $\text{Ni}_{0.1}\text{Mn}_{0.4}\text{Cu}_{0.2}\text{Cd}_{0.3}\text{Fe}_2\text{O}_4$ nanoparticles have been synthesized by following the sol-gel auto combustion process. Crystallite size and lattice constants have been calculated from XRD data. It has been observed that the experimental lattice constant value was estimated 8.466 Å, while the theoretical lattice constant value was estimated 8.342 Å. Surface morphology has been examined by TEM and FESEM micrographs. The average particle size has been derived from the histogram drawn from the FESEM image was found 42.5 nm. The presence of all elements has been confirmed by the EDS spectrum. From the two distinguished absorption bands noticed from the FT-IR spectrum, the formation of spinel ferrites has been confirmed. Intrinsic magnetization has been observed from the VSM data. Using VSM data, various parameters that are related to magnetization have been determined.

Keywords- Nanoferrites; Sol-Gel auto combustion method; TEM; FESEM; Histogram; VSM.

Date of Submission: 09-03-2020

Date of Acceptance: 23-03-2020

I. Introduction

For scientific and commercial use, spinel ferrites prove themselves as a potential candidate among all the ferrite materials used in the electronic world [1]. The properties of spinel ferrites vary due to their constituents, valence state, and their distributions of the cations. Based on the compositions and their distributions, structural and magnetic properties of the materials are changed. The general expression of spinel ferrite can be inscribed in the form AB_2O_4 , where in the place "A", various divalent ion, namely Ni^{2+} , Cu^{2+} , Cd^{2+} , Zn^{2+} , Mn^{2+} , Co^{2+} , Fe^{2+} , etc. can be added. In contrast, in the place "B", different trivalent ion such as Fe^{3+} , Mn^{3+} , etc. can be substituted. A^{2+} and B^{3+} cations can exist in the material either in the tetrahedral sites or octahedral sites based on their site preference. In normal spinel structure, the entire divalent ion occupies in the tetrahedral site, whereas in the inverse spinel structure, they are distributed in both tetrahedral and octahedral sites [2]. According to the cation distributions, the properties of nano ferrites are different from that of bulk materials [3, 4]. High resistive value and low eddy current loss make the nano ferrites material as a potential candidate for high-frequency devices [5]. Now, in the electronics world, size becomes very much essential properties due to its compactness; additionally, it becomes easier to use the materials for high-frequency applications [3]. Depending on the high magnetic performance, high resistivity, and low eddy current loss, nickel-based ferrites have now become the center of attraction [6]. By substituting other divalent ions in nickel-based ferrites, structural and magnetic properties can easily be tailored.

Sattar *et al.* synthesized $\text{Ni}_{0.6-t}\text{Mn}_t\text{Zn}_{0.4}\text{Fe}_2\text{O}_4$ and investigated the structural, magnetic, and electrical properties of the compositions. They found that the average grain size enlarges with the substitution of Mn ion, and they also observed improved magnetic properties simultaneously [7]. Venkataraju *et al.* synthesized $\text{Mn}_{(0.5-x)}\text{Ni}_x\text{Zn}_{0.5}\text{Fe}_2\text{O}_4$ via the chemical co-precipitation method. They found that both magnetization and Curie temperature decreases with the enhance of nickel ion except one composition [8]. Salah *et al.* prepared $\text{Mn}_{1-x}\text{Cu}_x\text{Fe}_2\text{O}_4$ ferrites ($0.2 \leq x \leq 0.5$) by the co-precipitation method. They observed a normal spinel structure by the Rietveld refinement method. They also found an increased lattice parameter and decreased crystallite size with the increase of copper ion. They also confirmed different chemical bonds by IR absorption spectra [9]. Though there is various synthesis techniques such as chemical co-precipitation, ceramic, sol-gel, microemulsion method [10-12] are used typically, but to achieve high-quality materials with minimal loss for high-frequency applications, sol-gel auto combustion technique is best for its low cost, facile synthesis technique, production time and homogeneity of the prepared sample.

In the current research, the optimized stoichiometry $\text{Ni}_{0.1}\text{Mn}_{0.4}\text{Cu}_{0.2}\text{Cd}_{0.3}\text{Fe}_2\text{O}_4$ has been chosen to study the structural and magnetic properties. No work has yet been reported on this material to study its properties. In this work, we aimed to prepare $\text{Ni}_{0.1}\text{Mn}_{0.4}\text{Cu}_{0.2}\text{Cd}_{0.3}\text{Fe}_2\text{O}_4$ by using the sol-gel auto combustion process. We

have primarily focused ourselves to determine the value of experimental and theoretical lattice constants, crystallite size, X-ray density, and other parameters specified from XRD data. The structural properties also have been studied by TEM, FESEM, EDS, and FTIR. In the present research, the magnetic properties have been examined by using VSM and calculated the saturation magnetization, remanent magnetization, coercivity, magnetic moment, and anisotropic constant values.

II. Experimental

2.1 Synthesis of nanoparticles

Nitrate salts of nickel, manganese, copper, cadmium, and iron have been used to synthesize $Ni_{0.1}Mn_{0.4}Cu_{0.2}Cd_{0.3}Fe_2O_4$ by the sol-gel auto combustion system. Firstly, all the salts were dissolved in ethanol (C_2H_6O), then using a magnetic stirrer; the solution was stirred continuously at 70 °C till gel form was noticed entirely. During this process, the pH of the solution was kept at a fixed value 7 by adding ammonia slowly. This mixture was kept in a water tub at 170 °C, and then the gel was heated at a temperature of 200 °C for five hours in the air. Finally, a fluffy powder obtained. To eliminate the impurity from the powder, this powder was heated at 700 °C for another five hours. Lastly, $Ni_{0.1}Mn_{0.4}Cu_{0.2}Cd_{0.3}Fe_2O_4$ nanoparticles were obtained that were subjected to examine various structural and magnetic properties.

2.2 Characterization

Philips X'Pert Pro X-ray diffractometer (PW3040) was employed to acquire X-ray diffraction (XRD) spectra at room temperature. Using Scherrer's formula, crystallite size has been calculated from the peak (311) by following formula [13]:

$$D = \frac{0.9\lambda}{\beta \cos\theta}$$

Here, crystallite size is D , X-ray wavelength (1.54 Å) is λ , full width at half maxima is β , and angle of diffraction is θ .

By the Nelson-Riley extrapolation method, the exact lattice parameter has been determined. The experimental (a_{exp}) and theoretical lattice constant (a_{th}) have been calculated from the subsequent formula:

$$a_{exp} = \frac{d_{hkl}}{\sqrt{(h^2 + k^2 + l^2)}}$$

$$a_{th} = \frac{8}{3\sqrt{3}} [(r_A + R_0) + \sqrt{3} (r_B + R_0)]$$

where d_{hkl} is the distance among two consecutive planes, R_0 is the radius of oxygen ion (1.32 Å).

Value of X-ray density (ρ_x) has been resolved by the following formula:

$$\rho_x = \frac{8M}{Na^3}$$

where the molecular weight is M , Avogadro's number is N , and lattice constant is a .

The ionic radii, bond lengths of tetrahedral and octahedral sites have been resolved via Standley's relations [14].

$$A - O = \left(u - \frac{1}{4}\right) a\sqrt{3}$$

$$B - O = \left(\frac{5}{8} - u\right) a$$

$$r_A = \left(u - \frac{1}{4}\right) a\sqrt{3} - r(O^{2-})$$

$$r_B = \left(\frac{5}{8} - u\right) a - r(O^{2-})$$

where lattice constant is a , radius of oxygen ion is $r(O^{2-})$ (1.35 Å) and u signifies parameter for oxygen ion.

The hopping length of the ferrite ions at the tetrahedral (L_A) and octahedral (L_B) sites were resolved by the subsequent method [15].

$$L_A = a \left(\frac{\sqrt{3}}{4}\right)$$

$$L_B = a \left(\frac{\sqrt{2}}{4}\right)$$

Employing transmission electron microscope (TEM) (Model: Talos F200S, ThermoFisher (FEI), US, operating voltage 200 kV), and field emission scanning electron micrographs (FESEM) (model JEOL-JSM 7600F, operating voltage 5 kV), the surface configuration of the ferrites have been inspected. FESEM has also outfitted with energy dispersive spectroscopy (EDS). By means of the linear intercept method, the average grain size has been estimated [16]. Applying operating voltage 10 kV, the EDS spectrum has been recorded. With the help of

the PerkinElmer spectrometer (model no. 8400S USA), the FTIR spectra of the ferrite samples have been recorded.

M-H curve has been recorded with a vibrating sample magnetometer (VSM) (EV-9, Microcense LLC, USA). Using the following relation, the value of the magnetic moment has been calculated:

$$\mu_B = \frac{M \times M_s}{5585}$$

where the molecular weight is M, and saturation magnetization is M_s .

III. Result And Discussion

3.1 XRD analysis

The XRD spectra of $Ni_{0.1}Mn_{0.4}Cu_{0.2}Cd_{0.3}Fe_2O_4$ nanoparticles calcined 700 °C at are represented in Fig. 1. Seven major peaks were obtained from the XRD spectrum, which confirms the cubic spinel structure along with single-phase. All the peaks have been verified by the JCPDS NO. 019-0692 XRD cards [17]. No impurity peak has been noticed in the spectrum. Broad XRD line indicates the nanosize of the particles.

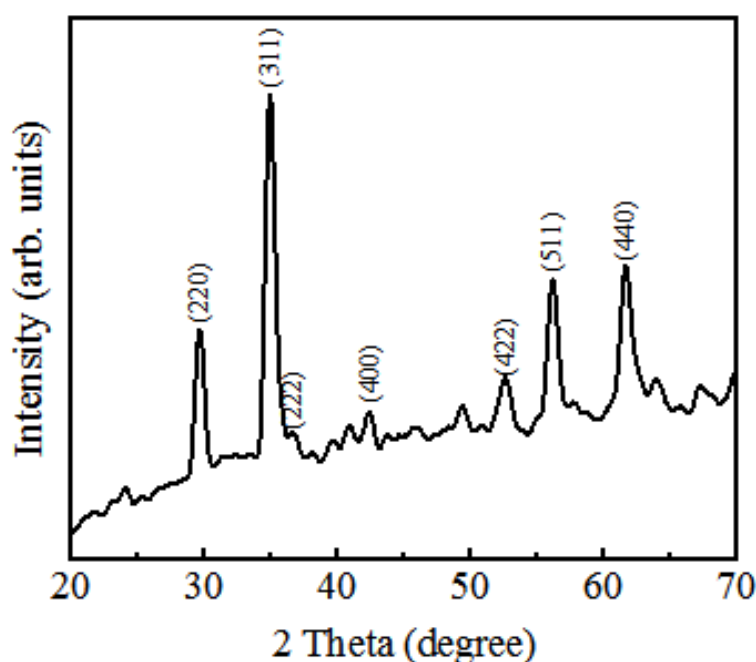


Fig. 1. XRD of $Ni_{0.1}Mn_{0.4}Cu_{0.2}Cd_{0.3}Fe_2O_4$ nanoparticles.

Various parameters obtained from XRD data have been tabulated in Table 1. It has been that the value of the investigational lattice constant is 8.466 Å, while the value of the hypothetical lattice constant is 8.342 Å. Theoretically, there is a defect in the powder sample, but experimentally it is not always true; that's why the value of experimental lattice constant is higher than that of theoretical lattice constant. The estimated crystallite size has been observed 36 nm. It was found X-ray density is 5.47 gm/cc. In Table 1, the estimated value of the ionic radius, bond length, and hopping length have been listed.

Table 1: Different parameters estimated from XRD for $Ni_{0.1}Mn_{0.4}Cu_{0.2}Cd_{0.3}Fe_2O_4$

Experimental Lattice Constant Å	Theoretical Lattice Constant Å	Crystallite Size nm	X-ray density ρ_x (gm/cc)	r_A Å	r_B Å	A-O Å	B-O Å	L_A Å	L_B Å
8.466	8.342	36	5.47	0.483	0.766	1.833	2.116	3.666	2.993

3.2 TEM analysis

The TEM images of $Ni_{0.1}Mn_{0.4}Cu_{0.2}Cd_{0.3}Fe_2O_4$ nanoparticles have been given for three magnifications in Fig 2.

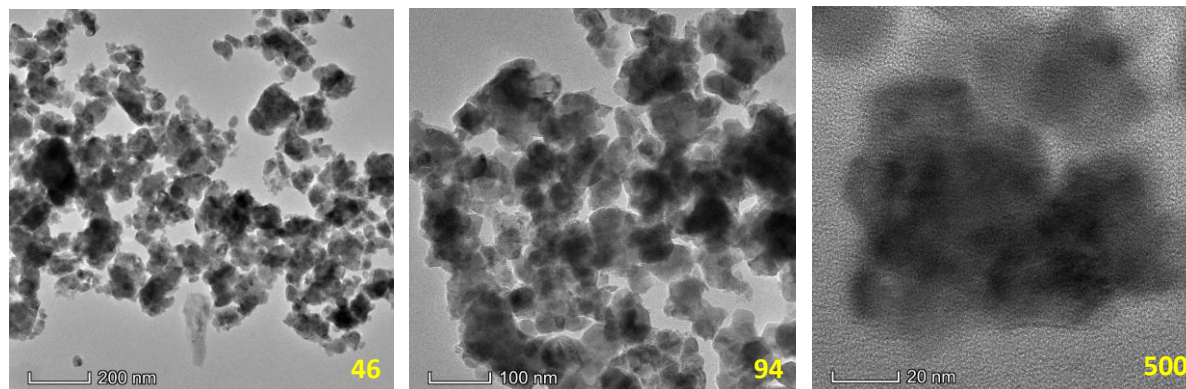


Fig. 2. High Resolution Transmission Electron Microscope (TEM) analysis of the prepared $Ni_{0.1}Mn_{0.4}Cu_{0.2}Cd_{0.3}Fe_2O_4$ nanoparticles at different magnifications.

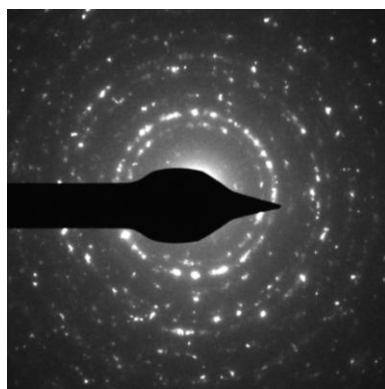


Fig. 3. Selective Area Electron Diffraction (SAED) pattern of $Ni_{0.1}Mn_{0.4}Cu_{0.2}Cd_{0.3}Fe_2O_4$ nanoparticles.

From the images, it has observed that the particle size is below 50 nm. Nearly spherical shaped particles have been noticed in the images. Slight agglomeration also has been seen in the images. The selected area electron diffraction (SAED) pattern has been given in Fig 3. The clear presence of diffraction planes confirms the formation of spinel ferrites.

3.3 FESEM and EDS analysis

FESEM micrographs of the $Ni_{0.1}Mn_{0.4}Cu_{0.2}Cd_{0.3}Fe_2O_4$ nanoparticles have been represented in Fig. 4. Nearly identical and consistent particles with fractional agglomeration have been observed. Due to the existing magnetic moment, this agglomeration takes place. The histogram that represents particle size distribution depicted in Fig. 5. It has been found that the average particle size is 42.5 nm that is comparable with the crystallite size computed from the XRD data.

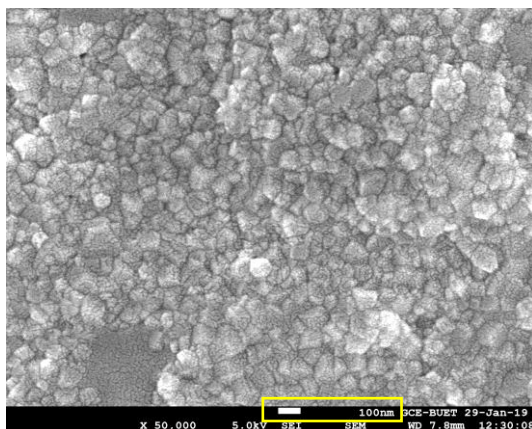


Fig. 4. FESEM micrograph ($\times 50,000$) of $Ni_{0.1}Mn_{0.4}Cu_{0.2}Cd_{0.3}Fe_2O_4$ sample

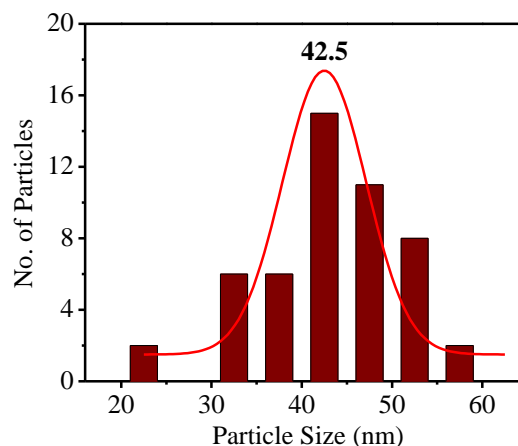


Fig. 5. FESEM micrograph ($\times 50,000$) of $Ni_{0.1}Mn_{0.4}Cu_{0.2}Cd_{0.3}Fe_2O_4$ sample

In Fig. 6, the EDS spectrum of $Ni_{0.1}Mn_{0.4}Cu_{0.2}Cd_{0.3}Fe_2O_4$ has been given. From EDS analysis, the purity of the ferrites sample has been proved. The amount of element and atomic percentages has been tabulated in Table 2. The proportions of the components exposed that there is no loss of elements has been noticed.

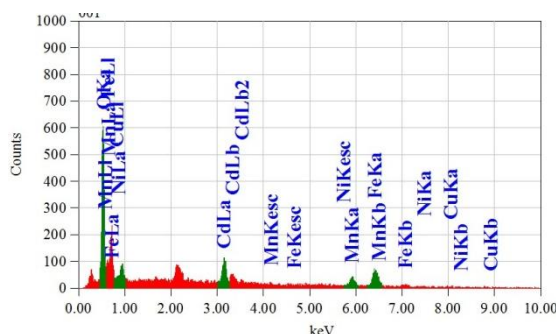


Fig. 6. EDS spectrum ($50,000\times$) of $Ni_{0.1}Mn_{0.4}Cu_{0.2}Cd_{0.3}Fe_2O_4$ sample

Table 2

The elements of each sample composition $Ni_{0.1}Mn_{0.4}Cu_{0.2}Cd_{0.3}Fe_2O_4$ nanoparticles analyzed by (% weight) obtained by EDS

	Ni	Cu	Cd	Mn	Fe	O
Element %	3.91(± 0.71)	2.47(± 0.18)	16.54(± 0.76)	14.48(± 1.40)	40.74(± 1.57)	21.85(± 3.23)
Atomic %	2.55(± 0.44)	1.49(± 0.07)	5.70(± 0.58)	10.27(± 1.60)	28.25(± 2.75)	51.74(± 4.88)

3.4 FTIR analysis

FTIR spectrum of $Ni_{0.1}Mn_{0.4}Cu_{0.2}Cd_{0.3}Fe_2O_4$ has been given In Fig. 7. Two absorption bands have been identified around 360 cm^{-1} and 590 cm^{-1} , which corresponds to the octahedral and tetrahedral group of spinel ferrites [18]. This change in two sites is due to the change in iron and oxygen bond length. The peak 1634 cm^{-1} indicates the bending of hydroxyl ion due to chemically absorbed H_2O . For C-H elongated vibrations, the crest 2924 cm^{-1} observed. For the stretching mode of vibration, the band at 3428 cm^{-1} has been found.

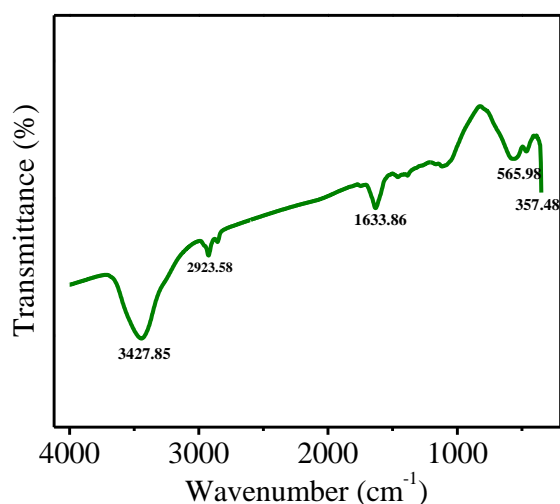


Fig. 7. FTIR Spectra of $Ni_{0.1}Mn_{0.4}Cu_{0.2}Cd_{0.3}Fe_2O_4$ as dried samples

3.5 Magnetic measurements

M-H curve of $Ni_{0.1}Mn_{0.4}Cu_{0.2}Cd_{0.3}Fe_2O_4$ has been given in Fig. 8.

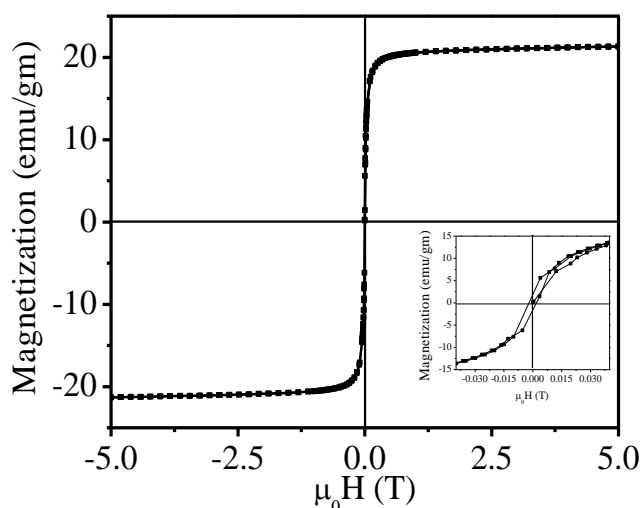


Fig. 8. Magnetic Hysteresis Loops of $Ni_{0.1}Mn_{0.4}Cu_{0.2}Cd_{0.3}Fe_2O_4$

Table 3: Magnetization data of $Ni_{0.1}Mn_{0.4}Cu_{0.2}Cd_{0.3}Fe_2O_4$

M_s (emu/gm)	M_r (emu/gm)	M_r/M_s	Coercivity (H_c) (T)	μ_B (Bohr magneton)	$K_1 = M_s H_c / 2$ $\times 10^4$ (erg/cm ³)
21.11	1.78	0.08	0.002	0.94	0.02

Using the curve, the value of various magnetic parameters have been computed and presented in Table 3. From the table, it has been observed that the value of saturation magnetization (M_s) is 21.11 emu/gm, remanent magnetization (M_r) is 1.78 emu/gm, coercivity (H_c) is 0.002 T, magnetic moment (μ_B) is 0.94 and the anisotropy constant (K_1) is 0.02 erg/cm³. The low value of coercivity confirms that the material is soft ferrite. The value of M_r/M_s reveals the existence of anisotropy within the sample.

IV. Conclusion

Nanoferrites $Ni_{0.1}Mn_{0.4}Cu_{0.2}Cd_{0.3}Fe_2O_4$ has been successfully prepared via the sol-gel auto combustion process. The structural and magnetic properties of the nano ferrites have been studied. By Scherrer formula, the calculated crystallite size was observed 36 nm, and X-ray density was found 5.47 gm/cc. Homogeneous particle structure with soft agglomeration was observed in both TEM and FESEM images. Spinel structure was validated by the SAED pattern. Elemental analysis was done by the EDS spectrum. The configuration of the spinel structure was also proved by the absorptions band found from the FTIR spectrum. Low coercivity value revealed that the sample is a soft ferrite. All the structural and magnetic properties enlighten the probability of the sample as a suitable candidate for high-frequency appliances.

Acknowledgment

The authors are obliged to Dept. of Physics, Chittagong University of Engineering and Technology (CUET), Chattogram-4349, Bangladesh, for the relentless support.

References

- [1]. S. Ahmed, S. Ogale, G. Papaefthymiou, R. Ramesh, P. Kofinas, *Appl. Phys. Lett.* 80 (2002) 1616-1618. <https://doi.org/10.1063/1.1456258>
- [2]. D. S. Mathew, R.-S. Juang, *J. Chem. Eng.* 129 (1-3) (2007) 51-65. <https://doi.org/10.1016/j.ccej.2006.11.001>
- [3]. V. Musat, O. Potecasu, R. Belea, P. Alexandru, *Mater Sci Eng B* 167 (2010) 85-90. <http://dx.doi.org/10.1016/j.mseb.2010.01.038>
- [4]. A. T. Raghavender, N. H. Hong, *J. Magn. Magn. Mater.* 323 (2011) 2145-47. <http://dx.doi.org/10.1016/j.jmmm.2011.03.018>
- [5]. K. M. Battoo, *Phys. B: Cond. Matt.* 406 (2011) 382-87. <http://dx.doi.org/10.1016/j.physb.2010.10.075>
- [6]. S. E. Shirsath, B. G. Toksha, R. H. Kadam, S. M. Patange, D. R. Mane, Ganesh S. Jangam, AliGhasemi, *J. Phys. Chem. Sol.* 71 (2010) 1669-1675. <http://dx.doi.org/10.1016/j.jpcs.2010.08.016>
- [7]. A. A. Sattar, H. M. El-Sayed, K. M. El-Shokrofy, and M. M. El-Tabey, *JMEPEG* 14 (2005) 99-103. <http://dx.doi.org/10.1361/10599490522185>
- [8]. C. Venkataraju, G. Sathishkumar, K. Sivakumar, *J. Magn. Magn. Mater.* 322 (2010) 230-233. <http://dx.doi.org/10.1016/j.jmmm.2009.08.043>
- [9]. L. M. Salah, A. M. Moustafa, I. S. Ahmed Farag, *Ceram. Inter.* 38 (2012) 5605-5611. <http://dx.doi.org/10.1016/j.ceramint.2012.04.001>
- [10]. R. Arulmurugan, B. Jeyadevan, G. Vaidyanathan, S. Sendhilnathan, *J. Magn. Magn. Mater.* 288 (2005) 470-477. <https://doi.org/10.1016/j.jmmm.2004.09.138>
- [11]. H. Yang, X. Zhang, W. Ao, G. Qiu, *Mater. Res. Bull.* 39(6) (2004) 833-837. <https://doi.org/10.1016/j.materresbull.2004.02.001>
- [12]. M. A. Dar, J. Shah, W. Siddiqui, R. Kotnala, *Appl. Nanosc.* 4(6) (2014) 675-82. <https://doi.org/10.1007/s13204-013-0241-x>
- [13]. B. D. Cullity, *Elements of X-ray Diffraction*, Addison-Wesley, London, 1959.
- [14]. J. Standely, *Oxide Magnetic Materials*, Clarendon, Oxford, UK, 1972.
- [15]. S. Mirzaee, S. F. Shayesteh, S. Mahdaviifar, *Polym.* 55(16) (2014) 3713-3719. <https://doi.org/10.1016/j.polymer.2014.06.039>
- [16]. T. J. Shinde, A. B. Gadkari, P. N. Vasambekar, *J. Mater. Sci. Mater. Electr.* 21(2) (2010) 120-124. <https://doi.org/10.1007/s10854-009-9878-3>
- [17]. Shamima Nasrin, F.-U.-Z. Chowdhury, S. M. Hoque, *Phys. B: Cond. Matt.* 561 (2019) 54-63. <https://doi.org/10.1016/j.physb.2019.02.053>
- [18]. J. Balavijayalakshmi, Greeshma, *J. Envir. Nanotech.* 2(2) (2013) 53. <https://doi.org/10.13074/jent.2013.06.132015>

M. Moazzam Hossen. "Variation of structural and magnetic properties of $Ni_{0.1}Mn_{0.4}Cu_{0.2}Cd_{0.3}Fe_2O_4$ prepared by sol-gel auto combustion process." *IOSR Journal of Applied Physics (IOSR-JAP)*, 12(2), 2020, pp. 35-41.